ISSN 1674-1056
http://cpb.iphy.ac.cn
http://iopscience.iop.org/cpb
中国物理 B
Chinese Physics
中国物理
Chinese Physics B

Wetting failure condition on rough surfaces

Feng-Chao Yang(杨冯超), Xiao-Peng Chen(陈效鹏)

Citation: Chin. Phys. B . 2019, 28(4): 044701. **doi:** 10.1088/1674-1056/28/4/044701
Journal homepage: http://cpb.iphy.ac.cn; http://iopscience.iop.org/cpb

What follows is a list of articles you may be interested in

A multicomponent multiphase lattice Boltzmann model with large liquid-gas density ratios for simulations of wetting phenomena

Qing-Yu Zhang(张庆宇), Dong-Ke Sun(孙东科), Ming-Fang Zhu(朱鸣芳)
Chin. Phys. B . 2017, 26(8): 084701. **doi:** 10.1088/1674-1056/26/8/084701

Experimental study on supersonic film cooling on the surface of a blunt body in hypersonic flow

Fu Jia, Yi Shi-He, Wang Xiao-Hu, He Lin, Ge Yong
Chin. Phys. B . 2014, 23(10): 104702. **doi:** 10.1088/1674-1056/23/10/104702

Molecular dynamics simulations of the nano-droplet impact process on hydrophobic surfaces

Hu Hai-Bao, Chen Li-Bin, Bao Lu-Yao, Huang Su-He
Chin. Phys. B . 2014, 23(7): 074702. **doi:** 10.1088/1674-1056/23/7/074702

Wetting failure condition on rough surfaces*

Feng-Chao Yang(杨冯超)[1], and Xiao-Peng Chen(陈效鹏)[1,2,†]

[1] School of Mechanics, Civil Engineering and Architecture, Northwestern Polytechnical University, Xi'an 710129, China
[2] School of Marine Science, Northwestern Polytechnical University, Xi'an 710072, China

(Received 1 November 2018; revised manuscript received 2 January 2019; published online 19 March 2019)

Wetting states and processes attract plenty of interest of scientific and industrial societies. Air entrainment, *i.e.*, wetting failure, on smooth plate in wetting process has been investigated carefully before. Liquid bath entries of "rough" silicon wafers are studied experimentally in the present work, and the air entrainment condition is analyzed specially with the lubrication theory. The roughness effects on the moving contact lines are therefore explored. The contact line pinning is found to be the main reason for the dynamically enhanced hydrophobicity of rough surface, which implies an effective microscopic contact angle of $\theta_e = \theta_Y + 90^\circ$ where θ_Y is the Young's contact angle of the material. Our results suggest that the solid surfaces can be considered as hydrophobic ones for a wide range of dynamic process, since they are normally rough. The work can also be considered as a starting point for investigating the high-speed advancing of moving contact line on rough surfaces.

Keywords: wetting failure, roughness, lubrication theory, contact angle

PACS: 47.15.gm, 47.55.dr, 47.85.mf **DOI:** 10.1088/1674-1056/28/4/044701

1. Introduction

Wetting phenomena and wetting processes are important for industry and in nature. Droplet's rolling on lotus leaf,[1] basilisk lizard's running on the surface of a pool,[2] shorebird's drinking water,[3] *etc*., attract great interest of scientists. Meanwhile, by using the wetting mechanism, one can massively print functional material on soft substrates in electric industry,[4] control the small robot through "smart" liquid metal,[5] and control the mixing in droplets as chemical vessels.[6] However, in the framework of fluid mechanics, severe theoretical challenge arises in analyzing the (liquid–air–solid) contact line motion on a solid surface due to the deduced shear stress singularity.[7,8] The assumptions of precursor film, non-Newtonian, and liquid evaporation, *etc*., were therefore made.[8] Coupling with slip boundary condition, the lubrication model is developed into a powerful tool to describe the dynamics of a moving contact line.[9] Marchand *et al.*[10,11] found that it can well predict the air entrainment condition when a smooth plate enters into viscous liquids vertically. On the other hand, the wall heterogeneity has been found to play important roles in determining the wetting states of liquids on a solid wall so far,[12–14] thus exerting a subtle influence on the spreading outcomes of a droplet impact onto a wall,[15] *etc*. As is well known, the detailed investigations are still lacking, and one still has a great enthusiasm for knowing how to model a rough plate in wetting processes for practical purposes. In this paper, we conduct the experiments to explore the roughness effects on the moving contact line dynamics. Well controlled wall surfaces and liquids are adopted following the previous experimental and numerical attempts on this subject. An empirical simple model is subsequently proposed.

2. Experiment

The experimental apparatus adopted in the present research is similar to that used by Marchand, Chan, and Snoeijer,[10,11] which is schematically depicted in Fig. 1(a). The releasing of the plate was controlled by a motor-string-guideway system to preserve fixed speed of the plate as it entered into the liquid bath vertically. The entering speed was calibrated through high speed video snapshots. In our experiments, water–glycerol (WG) and ethanol–glycerol (EG) solutions were used as the liquid phases with various mass fractions of the components. The viscosity of the solutions ranged from 2.8 mPa·s to 325 mPa·s, the density was around 10 g/cm^3, and the interfacial tension was in a range of 31 mN/m–71 mN/m. The properties of the solutions are listed in Tables 1 and 2. We used both smooth and "rough" silicon wafers as the plates. All the plates were oxidized for 2 hours to preserve uniform wettability on the surfaces, and the electron microscopy scanning (EMS) showed that they were covered by a thin SiO_2 film. On the smooth silicon wafers, the Young's contact angles (θ_Y) of WG and EG solutions were about 50° and 40° , respectively. Meanwhile, the "rough" silicon wafers were prepared following the standard Micro-Electro-Mechanical process.[16] Micron sized cylindrical pillars or square grooves were etched on the surface of silicon wafer for rough plates, and the geometries are illustrated in Fig. 1(c). Of course, for the grooved plates, the texture could

*Project supported by the National Natural Science Foundation of China (Grant Nos. 11472220 and 11872315).
†Corresponding author. E-mail: xchen76@nwpu.edu.cn
© 2019 Chinese Physical Society and IOP Publishing Ltd

be parallel or perpendicular to the water surface in the experiments. As we can see later, the orientation of the pattern causes an apparent difference when the same wafer is plunged into the liquid pools.

The "liquid-bath entry" processes of the plates were recorded by a MegaSpeed MS-75K camera at 2000 frames per second (Fig. 1(a)). When the plunging speed was smaller than a threshold, the front of the contact line will advance over the plate surface smoothly, and a stable meniscus could be observed (Fig. 1(b)). While the speed was higher than the critical value, the contact line was distorted. Air bubbles was shot from the apex of the distorted contact line in the circumstance (Fig. 1(b)). For all the plates we used, "rewetting" bridge could be found in the unstable advancing, which is similar to the observation of Marchand's.[10] Slight differences from those observed by Marchand *et al.* were observed merely because our liquids had much lower viscosity and higher interfacial tension. However, figure 2 shows that our data for smooth plates are consistent with previous publications.

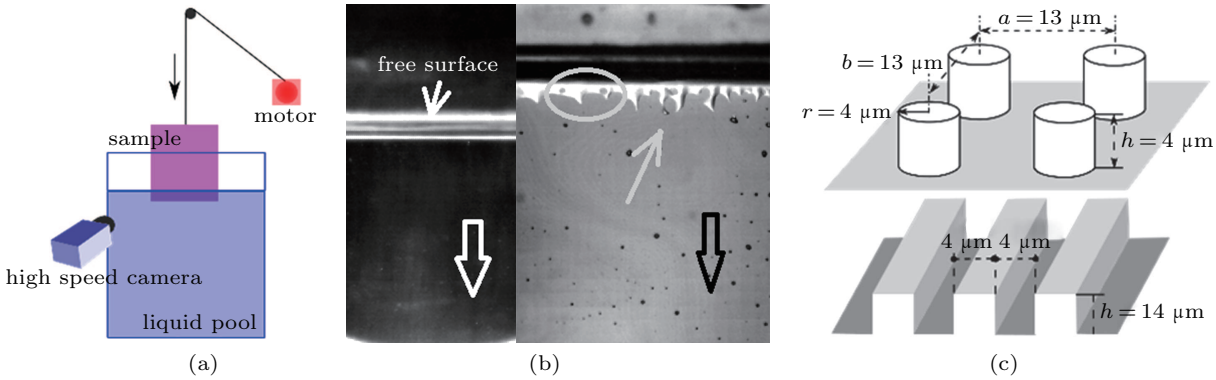


Fig. 1. (a) Experimental apparatus. (b) Plunging wafers into liquid bath with/without air entrainment, where the empty arrows indicate downward motion of plates. Left part: smooth wafer is plunged into water–glycerol solution with speed $U_p \approx 0.23$ (m/s), and contact line is stable. Right part: horizontally grooved wafer is plunged into the same solution with $U_p \approx 0.2$ (m/s), where contact line front is unstable. Solid arrow and circle denote bubble shot from apex of distorted contact line and "rewetting" bridges, respectively. (c) Geometries of etched microstructures on silicon wafer surfaces: cylindrical pillars (upper) and grooves (lower).

Table 1. Liquid properties, where θ_Y denotes the static contact angle on smooth surface; "M.F." the mass fraction of component (Comp.) A in solution; ρ, μ, γ denote density, viscosity, and interfacial tension of liquids, respectively.

Comp. A	Comp. B	M.F./%	ρ/(g/cm^3)	μ/(mPa·s)	γ/(mN/m)	θ_Y/(°)
Glycerol	water	30	1.07	2.8	71.0	50.9
Glycerol	water	50	1.13	6.6	70.0	49.4
Glycerol	water	70	1.18	29.0	67.0	50.0
Glycerol	water	85	1.22	109.0	64.0	52.2
Glycerol	water	95	1.25	325.9	62.0	51.7
Glycerol	ethanol	70	1.05	53.7	31.4	39.3
Glycerol	ethanol	75	1.07	111.4	34.2	39.4
Glycerol	ethanol	80	1.12	221.5	36.8	41.0

Table 2. Static apparent contact angle ($\theta_{A,r}$) values of various liquids on grooved silicon wafers, where "M.F." denotes mass fraction of component A in solutions.

Comp. A	Comp. B	M.F./%	$\theta_{A,r}$/(°)
Glycerol	water	30	34.7
Glycerol	water	50	34.7
Glycerol	water	70	35.0
Glycerol	ethanol	70	< 5
Glycerol	ethanol	75	< 5
Glycerol	ethanol	80	< 5

3. Results and discussion

3.1. Lubrication theory and preliminary experiments

For the cases of a smooth solid surface plunging into a viscous liquid, Snoeijer *et al.*[10,11] analyzed the meniscus in the vicinity of the moving contact line by using the lubrication theory.[9] In the later publication, the author proved that the theory can be applied to the flows in large contact angle. The governing equation is as follows:

$$\frac{\mathrm{d}^3 h}{\mathrm{d}s^3} = \frac{3Ca \cdot f(\theta, R)}{h(h+3\lambda_s)} + \sin(\theta - \alpha),$$
$$h(0) = 0, \quad \theta = \theta_e, \quad \theta(s \to \infty) = \alpha, \tag{1}$$

where s denotes the arc length, $h(s)$ the local thickness of the air film, and $\theta(s)$ the inclined angle of interface element (depicted in Fig. 3(a)). In the equation, the capillary number $Ca = \mu_L U_p/\gamma$, where U_p denotes the plunging speed of the plate. It is a dimensionless velocity characterizing the visco-capillary flow. The last term on the right-hand side represents the gravitational action, where α is the inclined angle of the plate and $\alpha = 90°$ in the present study. The function $f(\theta, R)$ evaluates the viscous effects of both phases, which is

expressed as

$$f(\theta,R)=\frac{2\sin^3\theta\left[R^2 f_1(\theta)+2Rf_3(\theta)+f_1(\pi-\theta)\right]}{3\left[-Rf_1(\pi-\theta)f_2(\theta)-f_1(\pi-\theta)f_2(\theta)\right]}$$

with

$$f_1(\theta)=\theta^2-\sin^2\theta,\quad f_2(\theta)=\theta-\sin\theta\cos\theta,$$
$$f_3(\theta)=\theta(\pi-\theta)+\sin^2\theta.$$

In the expression, $R=\mu_G/\mu_L$ denotes the viscosity ratio of the two phases, where the subscripts G and L denote gas and liquid, respectively. It is worth noting that the solution of Eq. (1) depends on two microscopic parameters, namely, slip length λ_s and microscopic contact angle θ_e. In practice, θ_e is usually set to be θ_Y on smooth surfaces, and λ_s to be an empirical value. In fact, we cannot measure λ_s directly experimentally, and the suitable value is obtained by fitting the predictions to the experimental results.

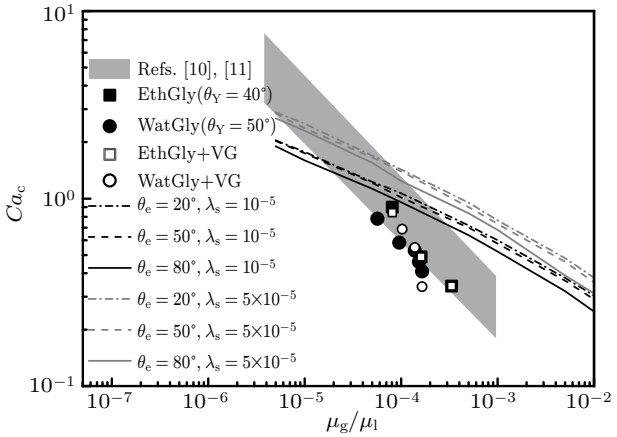


Fig. 2. Critical entry speed *versus* viscosity ratio for smooth plate (solid symbols) and that decorated with vertical grooves (empty symbols). Ethanol–glycerol (square) and water–glycerol (circle) solutions are used. Gray region shows the experimental data cited from Refs. [10] and [11]. Contact angle ($\theta_e=\theta_Y$) and slipping length (λ_s) are presented according to the lubricating theory (Eq. (1)). According to the comparison, results with $\lambda_s=10^{-5}$ are used as baselines for further analyses on rough surfaces.

Snoeijer's model successfully captures the most prominent features of the experimental results.[10,11] It leads to a solution of $\theta\equiv\arcsin(\mathrm{d}h/\mathrm{d}s)=\theta(s;\theta_e,Ca)$ with a maximum at some location: $\theta_{max}=\theta(s^*;\theta_e,Ca)$. The value of θ_{max} increases with Ca increasing, until $\theta_{max}=\pi$ is reached, which implies that the air might be entrapped,[10] *i.e.*, the wetting failure condition is reached. In our experiments, complex contact line front is observed when wetting failure occurs (see Fig. 1(b)). We solve Eq. (1) numerically by using Runge–Kutta and shooting method. For smooth silicon wafers, the predictions are consistent well with the experimental data qualitatively (see Fig. 2), and we also demonstrate the previous analyses.[10,11] On the other hand, by using a finite element method,[20] we find that equation (1) can predict the wetting failure conditions for two-dimensional cases (see the supplementary material). Therefore, we suppose that the deviation in Fig. 2 is due to the two-dimensional assumption in Eq. (1). In the latter analyses, we set the smooth plates results as baselines for both theoretical predictions and experiments respectively, and only care about the differences due to the roughness. Figure 2 shows the influences of both θ_Y and λ_s on the results in a reasonable range compared with the experimental results. Meanwhile, the critical speed decreases with θ_Y increasing or λ_s decreasing. In Fig. 2, we also present the results of experiment with using vertically grooved plate. It is interesting that the data are extremely close to the smooth plate ones. We then conclude that such a roughness has no effects on the wetting failure criterion in this circumstance. However, further experiments with horizontal microscopic patterns present different results. In the rest of the paper, we focus on the plates with horizontal grooves and micro-pillars, unless otherwise stated.

3.2. Experiments for rough surfaces

To characterize the roughness influence on wetting failure in detail, we try to model a rough surface with effective parameters for smooth surface. This idea is surely acceptable, since all theories for smooth surface are compared with (more or less) rough surface experiments. In Ref. [17], the authors found water entry cavity was induced easily as a rough hydrophilic sphere entered into water. They postulated that air was entrapped in the valley of the roughness when contact line advanced over the sphere surface. By using the Cassie–Baxter model,[12,14] a critical speed for splashing was estimated by following the Duez's procedure.[18] On the other hand, Qian and Wang[19] also derived an average value of the contact angle when the interface moves slowly on a chemically patterned surface, which was consistent with the scenario obtained from the Cassie–Baxter equation.

The geometry of the presented surface is regular enough and the corresponding effective contact angle under Cassie–Baxter (θ_{CB}) or Wenzel (θ_W) state could be obtained easily from the following equations[12,14]

$$\cos\theta_{CB}=\phi_s\cos\theta_Y+(1-\phi_s)\cos\pi,\quad\text{and}\quad\theta_{CB}>\theta_Y,\tag{2}$$
$$\cos\theta_W=r^*\cos\theta_Y,\quad\text{and}\quad\theta_W<\theta_Y,\tag{3}$$

where $\phi_s(\leq 1)$ is the fractional area of the solid-liquid interface per unit projected area under the liquid (see Fig. 3(b)) and the roughness factor $r^*\geq 1$. θ_e is then replaced by an effective contact angle (θ_{CB} or θ_W) instead of θ_Y in Eq. (1). Since it is already shown that the smooth silicon wafers are covered by a thin SiO_2 film and the surface of the substrate is hydrophilic, Wenzel state can be achieved by measuring the static contact angle (see Table 2). However, if θ_W is utilized in Eq. (1), then there will be $Ca_c(\theta_e=\theta_W)>Ca_c(\theta_e=\theta_Y)$. It contradicts our experimental observations (Figs. 1(b) and 4), which show the rough surfaces have lower critical entering speed than the

smooth ones. In Fig. 4, we compare the plates decorated with horizontal grooves and pillars with the smooth ones for both experiments and theoretical predictions. As a matter of fact, the most prominent features include that (i) the two rough plates have very close Ca_c values, (ii) Ca_c values of the two rough plates are lower than those of the smooth one. Then we suppose that air is entrapped in the valley of the grooves and use $\theta_e = \theta_{CB}$ (see Fig. 3(b)). According to Refs. [20] and [21] we also know the rough surface has a larger slip length, therefore $\lambda_s = 5 \times 10^{-5}$ is applied, which is slightly larger than that of the smooth one. However, it is shown that large deviation is found compared with the experimental results. Meanwhile, albeit $\lambda_s = 5 \times 10^{-5}$ is extremely empirical in Fig. 4, a larger one causes even worse prediction. Another clue for the real influence of roughness comes from feature (i). For the two topographies tested, the corresponding θ_{CB} values are obviously different from each other (see Eq. (2)), but they have almost the same Ca_c values. Therefore, the enhancement of wetting failure on rough surface cannot be yielded by any temporally or spatially averaged effect, namely the C–B state.

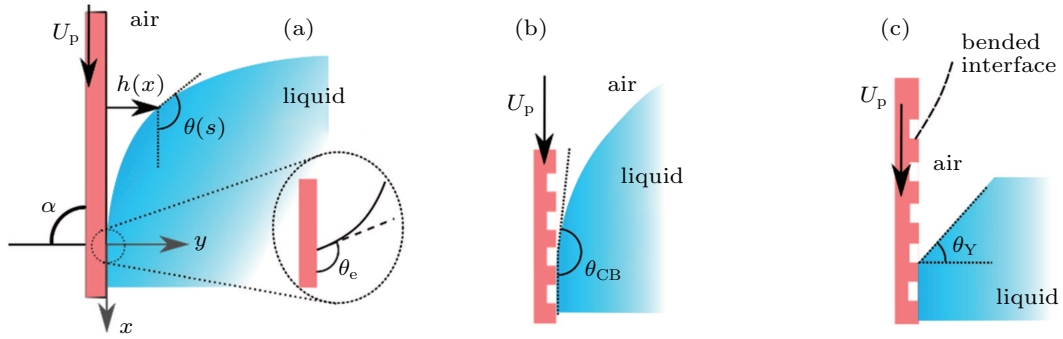


Fig. 3. (a) Illustration for lubrication theory. (b) Cassie–Baxter state when contact line advances on rough surface. (c) Contact line pinning and effective microscopic contact angle: $\theta_e = \theta_Y + 90^\circ$. Dashed curve indicates an imaginal bended interface.

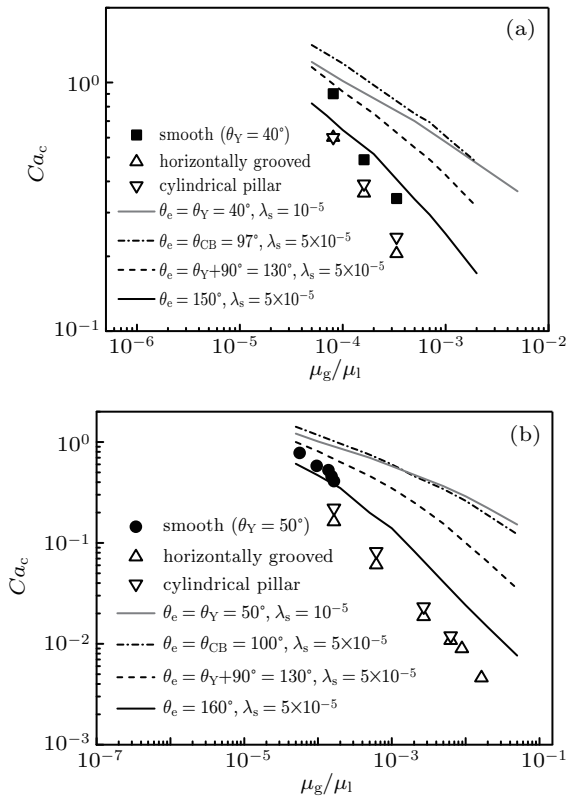


Fig. 4. Plots of critical entry speed *versus* viscosity ratio for rough plates. Experimental results and theoretical predictions for smooth surface are presented as baselines ($\lambda_s = 10^{-5}$). $\lambda_s = 5 \times 10^{-5}$ is applied in theoretical prediction (Eq. (1)) for rough plates. Although the latter is very empirical, a higher value leads to worse agreement with experimental result. (a) Liquids: ethanol–glycerol solutions. (b) Liquids: water–glycerol solutions. $\theta_e = 150^\circ$ and $\theta_e = 160^\circ$ in panels (a) and (b), respectively, indicate that $\theta_e > \theta_Y + 90^\circ$ is more reasonable for the predictions.

It is well known that "mesa" defects cause contact angle hysteresis, which could also be explained as energy barrier through thermodynamics.[12,14] The energy barrier will be overcome by adjusting the interface such that the contact angle reaches a new value while the contact line is pinned on the defect. As depicted in Fig. 3(c), a new value of the effective contact angle could be estimated a $(\pi/2 + \theta_Y)$. As shown in Fig. 4, given $\theta_e = (\pi/2 + \theta_Y)$, the lubrication theory provides reasonable predicts for both EG solution and WG solution. Furthermore, reminding the observations of rough plate with vertical grooves entering into the liquids, we can imagine that there are no energy barriers or pinning effects when the contact line advances along the grooves. So, the critical speed of such a rough plate is almost the same as that of the smooth surface. In Fig. 4, we further increase θ_e, which leads to better prediction. Probably, that is because of the slight bending of the interface as the contact line moves into the valley (see the dashed curve in Fig. 3(c)). By noting the above analyses, we again test several cases with $\lambda_s := 10^{-5}$–5×10^{-5} and $\theta_e := 130^\circ$–150°, and the current parameter set fits the experimental results better. Although it might not be the best, our results are still valid.

4. Conclusions and perspectives

In the present paper, we conduct water entry experiments of rough plates to explore the dynamic process of contact lines moving over rough surfaces. The flow in the vicinity of the contact line is well described with the traditional lubri-

cations theory. Unlike the equilibrium states, the dynamics of the moving contact line is governed greatly by local effect, namely pinning effect, rather than the temporal/spatial averages based on the thermodynamic approaches. The findings in our previous numerical simulations[20] are demonstrated. The experiments with various liquids and plate topographies show that the combination of local inclined angle of the valley and Young's contact angle of the liquid ($\pi/2+\theta_{\rm Y}$ in the paper) can be utilized as the effective microscopic angle, in order to evaluate the meniscus when the plate enters into the liquids. Coupled with an empirically increased slipping length, the critical speed for air entrainment, as the contact line advances on a rough surface, can be predicted. Of course, more detailed analysis of the slipping length influenced by roughness is still lacking. How the slipping length varies when the contact line pins on or releases from the defect is of great value.

Acknowledgment

We are grateful to Chan T S, Gao P and Thoraval M J for valuable discussion.

References

[1] Cheng Y T and Rodak D E 2005 *Appl. Phys. Lett.* **86** 144101
[2] Bush J W M and Hu D L 2006 *Ann. Rev. Fluid Mech.* **38** 339
[3] Prakash M, Quéré D and Bush J W M 2008 *Science* **320** 931
[4] Kumar S 2015 *Ann. Rev. Fluid Mech.* **47** 67
[5] Diebold A V, Watson A M, Holcomb S, Tabor C, Mast D, Dickey M D and Heikenfeld J 2017 *J. Micromech. Microeng.* **27** 025010
[6] Garcia-Cordero J L and Fan Z H 2017 *Lab A Chip* **17** 2150
[7] Huh C and Scriven L E 1971 *J. Colloid Intf. Sci.* **35** 85
[8] Zhao Y 2012 *Physico-Mechanics for surfaces and interfaces* (Peking: Science Press) (in Chinese)
[9] Eggers J 2004 *Phys. Rev. Lett.* **93** 094502
[10] Marchand A, Chan T S, Snoeijer J H and Andreotti B 2012 *Phys. Rev. Lett.* **108** 204501
[11] Chan T S, Srivastava S, Marchand A, Andreotti B, Biferale L, Toschi F and Snoeijer J H 2013 *Phys. Fluids* **25** 074105
[12] Quéré D 2008 *Ann. Rev. Mater. Res.* **38** 71
[13] Liu M and Chen X P 2017 *Phys. Fluids* **29** 082102
[14] Liu Y and Zhang X 2018 *Chin. Phys. B* **27** 014401
[15] Xu L, Barcos L and Nagel S R 2007 *Phys. Rev. E* **76** 066311
[16] Hao Y, Yuan W, Xie J, Shen Q and Chang H 2017 *IEEE Sen. J.* **17** 1246
[17] Zhao M H, Chen X P and Wang Q 2014 *Sci. Rep.* **4** 5376
[18] Duez C, Ybert C, Clanet C and Bocquet L 2007 *Nat. Phys.* **3** 180
[19] Qian T, Wang X and Sheng P 2006 *J. Fluid Mech.* **564** 333
[20] Yang F C, Chen X P and Yue P 2018 *Phys. Fluids* **30** 012106
[21] Philip J R 1972 *Z. Angew. Math. Phys.* **23** 353